ELSEVIER

International Journal of Mass Spectrometry 213 (2002) 45–62

www.elsevier.com/locate/ijms

Simulation of ion beam and optimization of orthogonal tandem ion trap/reflector time-of-flight mass spectrometry

C. Marinach[a], A. Brunot[a], C. Beaugrand[b], G. Bolbach[a], J.C. Tabet[a,*]

[a]*Laboratoire de Chimie Structurale Organique et Biologique, CNRS UMR 7613, Université Pierre et Marie Curie, Boite 45, 4 place Jussieu, 75252 Paris cedex 05, France*

[b]*MGP Instruments, BP 1, 13113 Lamanon, France*

Received 5 April 2001; accepted 30 July 2001

Abstract

The aim of the present work is to design an orthogonal coupling between a quadrupole ion trap and a reflector time-of-flight (reTOF) analyzer. According to the characteristics of the orthogonal ion injection in the reTOF analyzer, the incident ion beam properties have been determined. Different ion ejection modes from the trap cell, consistent with orthogonal-reflector time-of-flight mass spectrometry (O-reTOF/MS), have been investigated by simulations (SIMION 6.0) and experimental exploration. Especially, the following scanning modes have been studied: (1) dc scan applied to the ring electrode, (2) dc pulse applied to the ring electrode, and (3) dc pulse applied to the end-cap electrodes with switching off the drive rf voltage, under various storage conditions and for different *m/z* values. Distributions of ion velocities, kinetic energies, and ion ejection times, obtained by simulations and experiments, were compared using the ejection mode (2). Results from simulations of ions orthogonally injected into the reTOF/MS, show that the incident ion beam must be mono-energetic, with initial radial KE$<$2 eV to be efficiently deflected and detected. The simulations and experiments of original scanning from ion trap enlighten that dc ejection with rf voltage was not compatible with O-reTOF analysis (high energetic and noncontinuous ion beam). Appropriate dc ejection, with switching off the rf voltage, was consistent with O-reTOF analysis. For enhancing the duty cycle of the proposed system, the challenge is then to optimize ion ejection to get an ion beam as continuous as possible. (Int J Mass Spectrom 213 (2002) 45–62) © 2002 Elsevier Science B.V.

Keywords: Quadrupole ion trap; Time-of-flight; Kinetic energy measurements; Orthogonal coupling

1. Introduction

Rapid and accurate microbial identification is necessary, in monitoring potential contamination (e.g. in water and food) and most importantly for identifying bacteriological warfare agents. For such purposes, mass spectrometry (MS) is the most powerful analytical tool for analyzing a "signature" mass spectrum of chemical and biological materials. It is required to quickly identify related microorganisms, specific species, families, or particular strains, without ambiguity. For bacteriological identification, mass spectrometry has been used for the detection of defined biomarkers [1,2] such as lipids, carbohydrates, DNA, or proteins, and it offers many analytical advantages such as fast analysis, sensitivity, selectivity, and specificity. Electron impact ionization and chemical ionization mass

* Corresponding author. E-mail: tabet@ccr.jussieu.fr

PII S1387-3806(01)00508-5

spectrometry (more recently MAB [3]) coupled with pyrolysis techniques are well established methods for the elucidation of biomarkers [2,4]. More recently UV-matrix-assisted laser desorption ionization [5–7] and electrospray ionization [8,9] have seen fast growth as techniques suitable for such analysis. To create library data [10–13], the *m/z* range required for analyzing an efficient phospholipids fingerprint can be limited from 50 to 2 000 Th [4], with MS^2 scan, high resolution and mass accuracy of a few ppm. In addition, the mass spectrometer must be a field-portable instrument easy to use. Quadrupole filter and quadrupole ion trap (IT) are commonly used for such mobile mass spectrometers [14–16]. However, previous characteristics were not reached with these instruments.

The reflector time-of-flight mass spectrometry (reTOF/MS) has been shown to be quite efficient in such directions since its recent improvements have provided high resolution as well as accurate mass measurements [17]. The instrument size can be reduced [18,19] in order to be shipped on a vehicle. Nevertheless, when bacteria or viruses are analyzed, accurate mass measurements may be not sufficient and tandem mass spectrometry (MS/MS) experiments are required for the biomarker identification.

With the goal for obtaining previous characteristics, the combination of two analyzers in tandem can be considered such as a quadrupole filter or a quadrupole ion trap combined with a reTOF/MS. The former coupling has been done [20], and is already commercially developed with an orthogonal geometry. Determination of the *m/z* values were carried out with a mass accuracy of less than 10 ppm within a high resolution of 10 000 [21] at 6 000 Th. Such properties are essentially due to the orthogonal injection of ions into the source of TOF/MS [22]. Nevertheless, these instruments are essentially used for single-MS and MS/MS modes and are not easily shipped on a vehicle.

A noncommercial instrument, the orthogonal linear ion trap/TOF/MS [23] has shown interesting results in terms of sequential experiments, resolution, and mass accuracy measurements. However, nowadays this system is limited by the absence of a reflector on the

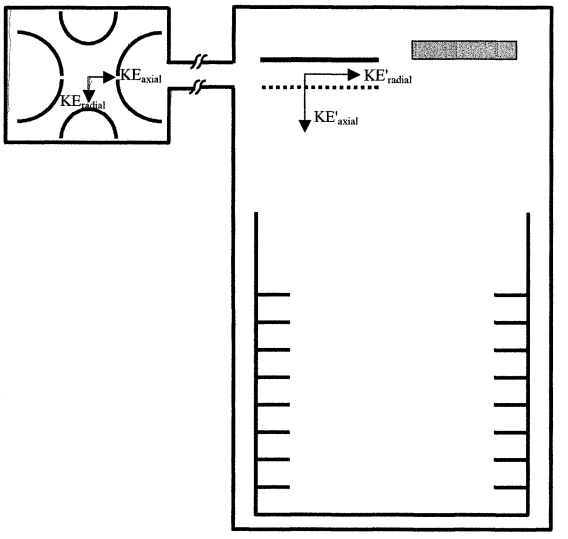

Fig. 1. Schematic view of the orthogonal coupling IT/O-reTOF/MS. The KE are indicated within the different references: KE for ion trap reference, KE′ for reTOF reference. In this coupling $KE_{axial} = KE'_{radial}$.

TOF/MS and MS^n scanning with such linear ion trap. The "in-axis" coupling of a quadrupole ion trap with a reTOF/MS has already been studied [24–30] and the results obtained with those instruments were encouraging. Resolution of 6 000 at 1 347 Th can be easily achieved, with a mass accuracy in the range from 100 to 500 ppm [30].

In an ion trap cell, the size of ion cloud is roughly 1 mm in diameter [28,31,32], with an optimized choice of the ion trapping voltage on the ring electrode. In the previous coupling in-axis quadrupole ion trap/reTOF/MS, ions are ejected by turning off the driving rf voltage and by applying a dc pulse voltage to end-caps (symmetrical or not). From such in-axis tandem, ejected ions will be characterized by time spread as well as broad spatial and velocity distributions, giving rise to an inefficient simultaneous analysis of all ions in the reTOF/MS. To improve resolution and mass accuracy measurements, an orthogonal ion injection can be chosen as an alternative. Indeed, the ion radial velocity distributions outside of the ion trap are weaker than the axial one. In the orthogonal injection source of the reTOF analyzer (O-reTOF), this radial distribution will be converted into axial

distribution for the O-reTOF analyzer (see Fig. 1) and will be easier compensated by the reflector system. The axial distributions of ion velocities outside ion trap are converted into radial distribution for the O-reTOF system which can lead to ion losses.

In the case of a nonsampling O-reTOF analysis, ions leave the ion trap and have to be simultaneously analyzed by the reTOF analyzer. This instrument requires specific and simultaneous conditions for high resolution. In such experiments, it can be assumed that (1) all ions have to be focalized in "space" and in "time" in orthogonal injection source to efficiently inject all ions in the reTOF/MS by applying a dc pulsed voltage on extraction lens and (2) the ion velocity must be consistent with a reTOF geometry and voltages, to involve efficient detection. These conditions could not be reached by ion ejection scanning at the natural $\beta_z=1$ boundary, because the average kinetic energy (KE) of ejected ions would reach 3 keV [33] for ions of 500 Th. In addition, the method of turning off the driving rf voltage followed by application of a dc voltage pulse to end-caps [24–29] did not permit the first reTOF condition to be reached. In fact, using these two ejection modes, the concerned ions cannot be simultaneously focused through the orthogonal injection source; indeed, ions of lower *m/z* ratios promptly leave ion trap cell with the highest velocity and larger ions are ejected with delay with the lowest velocity [33]. Consequently, sufficient focalization, in space and in time, cannot be achieved. Moreover, the average KE of ejected ions [33] is not consistent with O-reTOF analysis, since one can easily calculate that the extraction voltage would be higher than 100 kV.

Todd [34] and recently, Patterson [35] reported a dc scan mode that can be used for such orthogonal coupling: ions are ejected at the $\beta_z=0$ boundary by a dc ramp applied to the ring electrode or to the end-caps. Indeed, by increasing the dc voltage, the low *m/z* ions are first ejected with low velocity, and reciprocally for the delayed higher *m/z*. One could expected that, using well-chosen trapping parameters, the last ejected ions would catch up the first ones, and a focused region will be defined with ion velocity consistent with O-reTOF analysis.

In the case of a sampling analysis using pulsed technique on O-reTOF extraction lens, the velocity condition is also necessary. This requires an optimization of (1) voltages for all ion ejection from ion trap, getting a pseudocontinuous beam, and (2) of the duty cycle of the quadrupole IT/O-reTOF/MS.

The aim of our work is to design an orthogonal coupling between quadrupole ion trap and reTOF analyzers (see Fig. 1: IT/O-reTOF/MS). With the particular properties of these instruments, described previously, different modes of ion ejection from quadrupole ion trap to reTOF have been studied. The compatibility with the reTOF analysis have been explored by using SIMION 6.0 [36] and Visual basic 5.0 softwares. Ion ejection from the ion trap will be considered using dc scan, without scanning the driving rf voltage, or with dc pulse applied to end-cap electrodes after switching off the drive rf voltage. In order to verify simulations, these scanning modes were then applied to a commercial quadrupole ion trap. Experiments on the time and KE distributions of various ions, ejected from ion trap according to various modes, have been carried out and preliminary results are compared to the simulations.

2. Experimental

2.1. Ion trap scanning mode

Experiments were performed on a Varian Saturn III gas chromatography GC/MS (Varian, Palo Alto, CA). All data were taken on ions derived from perfluorotributyl amine (FC-43), ionized by electron impact and examined under standard ion trap conditions of He pressure (10^{-4} torr, but estimated to be an order of magnitude higher [37]) and temperature (150°C). The analytical scan used (Fig. 2) was similar to those previously described [37,38]. This analytical scan was controlled by the use of Varian QISMS 1.5 software coupled with Revision C Saturn software. The FC-43 ion scan function consisted of five time periods. During period (a), FC-43 was ionized and the rf level was set so that ions above 20 Th had stable trajectories and were stored. Period (b) corresponds

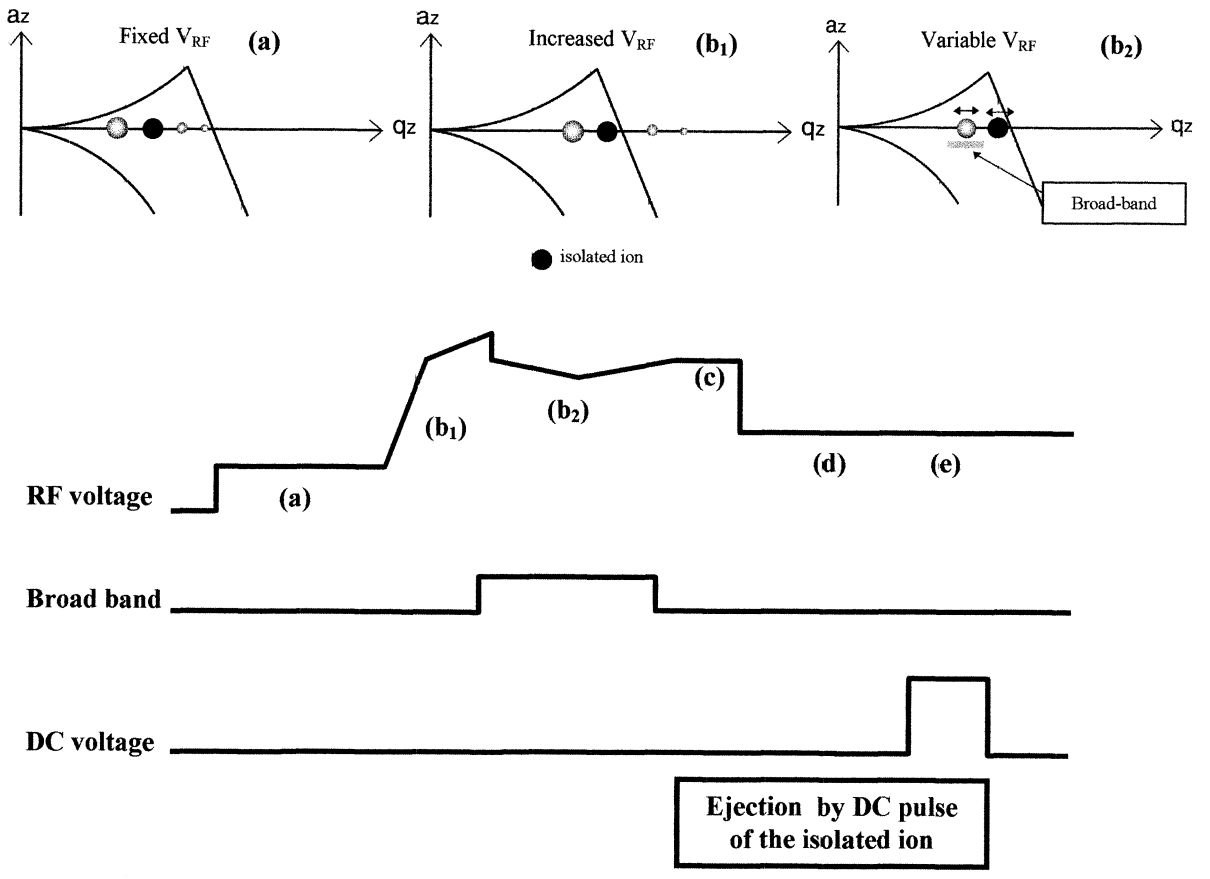

Fig. 2. Analytical scan used on the ion trap to eject an isolated *m/z* ion by a dc pulse voltage applied on the ring electrode: (a) ionization step at LMCO of 50 Th, (b) ion isolation, (c) KE cooling, (d) positioning the ion of interest at the desired working point and KE cooling, and (e) ion ejection.

first (b_1) to the isolation of the FC-43 diagnostic ion (e.g., *m/z* 69, *m/z* 131 or *m/z* 502) by a linear increase of the rf voltage to a lower value of the considered *m/z*, with a simultaneously application of an axial modulation (2 $V_{p\text{-}p}$ amplitude) to the end-cap electrodes. In the second part (b_2), the high *m/z* ratio ions were eliminated by applying a supplemental broad-band waveform voltage to end-caps (~30 V). The isolated ions were then cooled [period (c)] during 5 ms. Period (d) corresponded to the decrease of the rf level at the desired q_z value and the ion cooling at this value (4 ms). The ions were then ejected by a dc voltage (U_{dc}) applied to the ring electrode [period (e)]. The dc pulse voltage, which corresponds to the $\beta_z=0$ ejection, was calculated using QISMS software, and the used values for each q_z and *m/z* were reported in Table 1.

2.2. Ejected ion: kinetic energy and time distribution studied by retarding potential

A grid has been implemented between the exit end-cap and the detector (channeltron), on which a retarding potential was applied. Positive ions were ejected by applying U_{dc}, whereas end-cap electrodes were grounded. When grid was grounded, all transmitted ions were accelerated between the grid and the detector. As the grid potential was increased (supplied

Table 1
Experimental values of dc pulse voltage used for the ion ejection, according to the different *m/z* ratios and q_z values; these dc values were calculated by using QISMS software

m/z 69		*m/z* 131		*m/z* 502	
q_z	dc voltage (V)	q_z	dc voltage (V)	q_z	dc voltage (V)
0.85	156	0.88	315	0.46	355.5
0.74	120	0.78	251.4	0.41	276.3
0.63	89	0.67	187.4	0.35	201.9
0.53	63	0.56	131.8	0.29	140.8
0.42	40.6	0.44	85.3	0.23	90.4
0.32	23	0.33	48.4	0.17	51.0
0.21	10.3	0.22	21.6	0.14	35.5
0.10	2.58	0.11	5.4	0.12	22.7

by a home made 0–2 kV power supply), only ions with KE in excess of the value established by the grid potential were transmitted. Ion signal was recorded via an oscilloscope (Lecroy, Chestnut Ridge, NY) triggered by a signal related to U_{dc}. For each q_z, *m/z* and U_{dc} parameter triplet, intensity of the ion signal as a function of grid potential was derived to obtain KE distributions, and velocities were calculated for each *m/z* value. For each measurement, 1 000 scans were averaged for each grid potential step to obtained a significant statistic. Note that SIMION simulation of the iso-potential distribution of the implemented grid showed that the penetration field of the detector could be neglected. The same method was used to study ion ejection time, by keeping the grid potential to ground, and varying each q_z, *m/z*, and U_{dc} parameters. The measured ejection time included the time t_1 to eject the ion out from the cell (between start of the dc pulse voltage applied to the ring electrode and exit end-cap) and the time of flight t_2 for reaching the detector. The time t_2 (typically 1 to 3 μs) is much lower than t_1 (up to a few hundred of μs as measured in this study) and it can be neglected.

3. Method for simulations

Simulations were carried out using the main characteristics of both the quadrupole ion trap Saturn III GC/MS and reTOF/MS analyzers. The program SIMION 6.0 [36] was used to achieve quantitative and qualitative information about the influence of experimental parameters on ion motion.

3.1. Reflector time-of-flight simulations

The reTOF/MS (prototype from Bruker-Franzen Analytic, Bremen, Germany) was modeled in SIMION 6.0 using geometry provided by the constructor. The values of the different distances were confirmed. Physical characteristics of reTOF (Fig. 3) were included in the simulation, i.e. grid less and out of axis (~3° angle) two stage reflectron, grid less Wiley–McLaren source [39], deflection plates, field free region of ~1 m and detector (dual micro-channel plates, ϕ=25 mm). High precision of the 2D matrix in SIMION was used to provide accurate calculations of the ion motions. In the simulations, ion population (such as *m/z* 50, 100, 200, 500, 1 000, and 2 000) was generated around the center of the first extraction region with different initial radial KE. Constant initial conditions of the ion beam were KE_{axial}=0 eV, Δz=2 mm, Δr=10 mm (see Fig. 3). For each KE_{radial} step, deflection plate voltage was adjusted to efficiently detected the ion beam.

3.2. Ion trap simulations

The 3D-quadrupole ion trap was modeled in SIMION. The internal dimensions of the ion trap were those characterizing a stretched geometry with r_0=1.000 cm, z_0=0.783 cm, where z_0 represented the

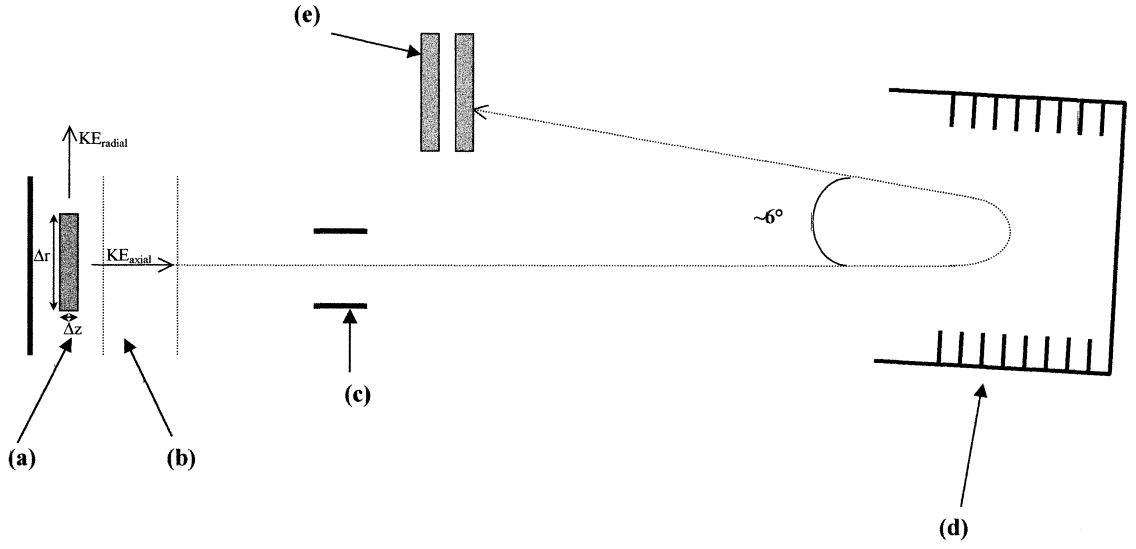

Fig. 3. Geometry out of axis (angle ~6°) of the two stages gridless ReTOF. Length of the drift region: ~2 m (a) was the first acceleration stage ($V_{acceleration}$ = 1 kV was applied on the first electrode), (b) was the second acceleration stage, (c) were the deflection plates, (d) was the gridless electrostatic mirror, and (e) was the detector.

half of the shortest distance between the two end-caps, and r_0 the radius of the ring electrode. Three electrodes were included in this simulation. The hyperbolic internal surface shape of the quadrupole ion trap was mathematically defined using a geometry file, provided by SIMION 6.0. In the simulation presented in this work, one grid unit in the 2D matrix corresponded to 0.100 mm in the real ion trap. This high precision ensured very accurate calculations of the ion motion inside ion trap. The ion positions (along the x, y, z axis) and velocities were calculated via a high-density matrix by SIMION program. Because of the low number of ions used in this simulation (<150 ions), ion-ion repulsion yielding space charge effects, as well as resulting effects due to the presence of nonlinear resonance (NLR), were not taken into account in the present simulations [40]. SIMION user program software considered two different models for the ion-cooling step: (1) linear damping and (2) velocity damping. The last model is the most appropriate in the high KE limit [41], and it was used for the simulations herein described. According to Forbes et al. [42], the results obtained with this model could be compared to those provided by ITSIM [43], and the mean free path of ions used in SIMION could be associated to both the buffer gas pressure and collision cross section. By using these results and home calculations, it has been found that a mean free path close to one correspond to a pressure of 10^{-3} Torr and a collision cross section of 500 Å^2, typically expected for ion size of 100 Th and He buffer gas, as in our experiments.

3.2.1. Ion generation and cooling

In order to simulate the ion extraction process, population of 120 single positive ions was generated in the 50–200 Th range (40 ions of 50, 100, and 200 Th) and in the 500–2 000 Th range (40 ions of 500, 1 000, and 2 000 Th). SIMION program generated randomly ions around the geometrical center of ion trap and the initial conditions were reported in Table 2. Due to the ion generation conditions, ions had a broad KE distribution. Before the ejection step, KE cooling with buffer gas was required. Thus, duration of the cooling step (t_{toc}) was included in these simulations. First simulations (not reported herein) on the initial ion KE and the cooling duration, shown that a duration of 300 μs was required to get the ion KE

Table 2
Initial conditions of one single ion for the SIMION 6.0 simulations; MFP is the mean free path; Integration time is T/100 where T is the drive rf period

MFP	1
P_{He} (Torrs)	10^{-3}
Z_{min} (mm)	−0.1
Z_{max} (mm)	+0.1
r_{min} (mm)	−0.1
r_{max} (mm)	+0.1
KE_{min} (eV)	0.005
KE_{max} (eV)	0.945

relaxation from initial average KE of 0.05 eV, with a broad KE distribution from 0 to 0.1 eV. These results were consistent with those published by He and Lubman [40] and by Forbes et al. [42]. The former [40] demonstrated that a relaxation time of 200 μs, was required for cooling ions of initial KE of 25 eV. Simulation of ion storage [41] demonstrated that 400 μs were required for cooling ions carrying out initial KE of 15 eV. Alternatively, Forbes et al. [42] have shown that 200 to 1 000 μs were required for cooling a single ion, depending upon the conditions used for simulations. The difference between all these simulations was likely due to different chosen initial parameters, or different models of the ion cooling (a 3D ion neutral hard-sphere model [40], the Langevin collision theory [44,45], and velocity damping model [36]). Moreover, the size of the ion cloud depended upon the storage conditions: at q_z=0.04, before cooling it was larger than that at q_z=0.8 [28,31] and thus, ion trapping was much less efficient. This resulted from the depth of the pseudopotential well [46] which was less deep at q_z=0.04, and the cooling step will be longer than that needed at q_z=0.8. To be sure that ion cloud was kinetically cooled prior to the ejection step, the cooling duration t_{toc} was fixed at 1 000 μs for all simulations.

3.2.2. rf and dc potentials

Potential $\Phi_0(t)$ applied to the ring electrode was controlled by the user program. The function that described this potential was given by:

$$\Phi_0(t) = U_{dc}(t) + V_{rf}\cos(2\pi ft + \Theta_0) \quad (1)$$

where V_{rf} was the driving rf voltage amplitude, f was its frequency (set to be fixed at 1.05 MHz), Θ_0 was the initial rf phase (set to be 0), and U_{dc} (t) was the dc voltage amplitude. These simulations reported the results on the following ion ejection mode: (1) a linear dc ramp $U_{dc} = \alpha t$, (2) a dc pulse $U_{dc} = U_0$, and (3) a dc pulse applied to end-caps by switching off the rf voltage $U_{dc} = 0$ and U_a and U_b to end-caps. Three dc ramps were studied in case: (1) α = 10 000, 5 000, and 1 000 V/s. For simulating dc pulse ejection (2) experimental values (Table 1) were used. In (3), after switching off the rf voltage, a dc pulse voltage was applied to the end-caps electrodes. Same voltage with opposite polarity was applied to these two electrodes, to have a relative low ion beam divergence from the cell exit [28].

In these simulations, t_{toc} (cooling duration) was used as the starting time of the dc voltage. Before this delay time, ions were kinetically cooled by collisions with the buffer gas (helium). The user program for simulating the trapping and the ion ejection controlled the amplitude of the potentials applied to the ring electrode and to the end-cap electrodes, and thus the scan rate α, t_{toc}, U_{dc}, U_a, U_b, and V_{rf} could be adjusted. Ejection time and ion velocity were recorded when the ion passed through the hole of the exit end-cap.

3.2.3. Trajectory overlapping calculations

The knowledge of ion ejection time and velocities allow us to study a possible overlapping of ion trajectories after ion trap ejection. This trajectory overlapping was calculated by a homemade program (Microsoft Visual Basic 5.0) using both results of simulation and experimental data. This program allows us to search for extension of overlapping in a field free region at different time after ejection and/or at different distance from the end-cap exit. The radial velocity was not taken into account in this calculation.

4. Results and discussion

4.1. Conditions on reflector time-of-flight analyzer

For analyzing simultaneously all the ions in the orthogonal injection mode, the reTOF instrument

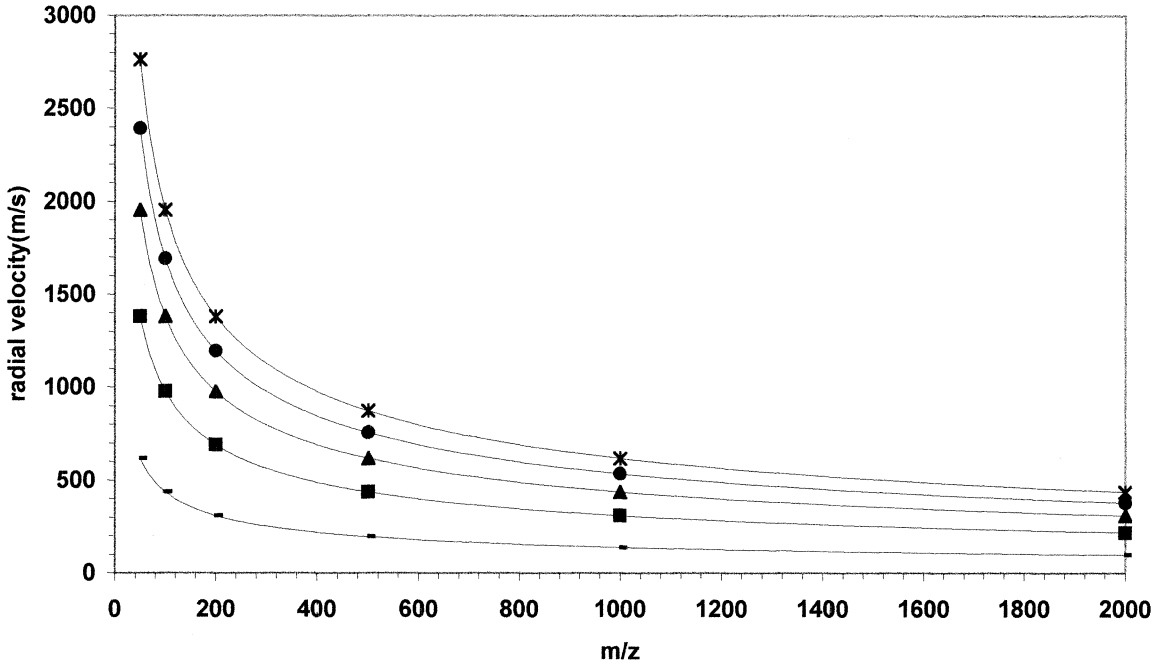

Fig. 4. Initial radial velocity allowing the reTOF/MS analysis as a function of the *m/z* ratio (axial acceleration 1 kV) and for different deflection plate voltages (simulations): (—) +10 V (voltage on deflection plate) for 1 eV (as initial radial KE), (■) +25 V for 0.5 eV, (▲) +44 V for 1 eV, (*) +50 V for 1.5 eV, and (×) +60 V for 2 eV.

requires particular conditions allowing high resolution and accurate mass measurements. Especially, (1) the ion cloud must be focalized in space and in time into the extraction volume of reTOF and (2) the ion velocity must be consistent with both the geometry and voltages of reTOF/MS. Only the last condition was required in the case of a sampling analysis. The out of axis (~3° angle) geometry of the two stage gridless reTOF was used to get the range of initial radial velocity (with respect to TOF axis) of ions in the extraction source (Fig. 3). This geometry and the voltages commonly applied for the gas analysis were simulated with SIMION software to achieve the useful KE range consistent for detection and high-resolution measurements. Fig. 4 shows the average radial velocities allowed for reTOF analysis versus the *m/z* ratios for different deflection plate voltages. The ion extraction voltage was set to 1 kV. The best resolution and mass accuracy were found as expected for a average radial KE close to 0 eV, and a low KE spread of 0.5 eV, due to the detector size (microchannel plate, ϕ = 25mm), whatever the *m/z* value in the 50–2 000 Th range. In addition, deflection plate voltage must be adjusted to compensate higher radial initial KE values. For example, an average radial KE of 0.1 eV was compensated by a potential of +10 V applied to one of the deflection plate. Limitation on available average KE was due to the maximal deflection voltage that can be applied (+60 V in the present case). The conclusion of these simulations was that the ion cloud might be effectively detected if the radial KE value of the ions is lower than 2 eV ($V_{deflection}$ = 60 V) with a KE spread of 0.5 eV, depending upon the deflection plate voltage. In the present orthogonal tandem coupling, the ion axial KE at the ion trap exit must be the same than that of the initial radial KE value in reTOF (see Fig. 1). Thus, the second condition (i.e., (2)) for performing reTOF analysis was obtained if all the ions leave the ion trap with a similar KE, in the range 0–2 eV (KE spread of 0.5 eV).

4.2. Condition on ion trap: ion ejection velocity and kinetic energy

Parameters such as the q_z working point for the different ejection modes, dc scan rate for dc ramp, and their influence respectively on ion velocities, have been studied in a *m/z* ratio range from 50 to 2 000 Th, keeping in mind the specific conditions for the O-reTOF analysis.

Within the adiabatic approximation of the Dehmelt pseudopotential well (i.e. $q_z<0.4$), the ion motion can be described by a two-dimensional harmonic motion of ions in a parabolic pseudopotential well having as components, the D_z and D_r depths in the z and r directions [46], respectively:

$$D_z = -q_z V_{RF}/8 \quad (2a)$$

$$D_r = D_z/2 \quad (2b)$$

For low q_z values, the pseudopotential well is not deep, and the ion cloud can be inefficiently trapped. From these trends, influence of different q_z values on the ion trapping has been studied as well as the average velocity of ions ejected out from the ion trap. For all the simulations, the t_{toc} value was set to 1 000 μs (see previous).

4.2.1. Simulations

Fig. 5 illustrates the influence of the q_z working point value on the average axial velocity of ions ejected by using a dc ramp [see Sect. 3.2.2. case (1)]. The simulations were done with different dc ramps (Fig. 5). At $q_z < 0.01$, ions of 200 Th were inefficiently trapped, due to a too weak pseudopotential well. Figs. 5(a) and 5(b) indicate that the decrease of trapping q_z values allows to reduce the average velocity of ions. The ions studied are ejected with an average axial velocity roughly proportional to the q_z value, for the set of the considered ions. Moreover, these ion velocities are roughly independent upon the dc ramp [Fig. 5(b)]. Fig. 6(a) shows that the average axial kinetic energy of ejected ions is a function of both the q_z and *m/z* values. From these values, a relationship between $KE_{z,ejec}$ (average axial kinetic energy of ions at the exit of ion trap), q_z and *m/z* can be deduced

$$KE_{z,ejec} = A\frac{m}{z}q_z^2 + Bq_z \quad (3)$$

In the first term, the A value is quite constant and is equal to 1.53 ± 0.3 eV/Th. This result can be compared to the theoretical calculations of the pseudopotential well depth [46]:

$$D_z = -\frac{m\Omega^2 z_0^2}{16ze}q_z^2 \quad (4)$$

with

$$\frac{\Omega^2 z_0^2 10^{-3}}{16eN} = 1.73 \text{ eV/Th} \quad (5)$$

where *N* is the Avogadro number, Ω is the pulsation of the driving rf voltage (f = 1.05 MHz), and z_0 is the half of the shortest distance between the two end-caps (z_0 = 0.783 cm). The value calculated from Eq. (5) is consistent with the A value determined from Eq. (3). The term B in Eq. (3) depends on the *m/z* value and the dc ramp voltage. It corresponds to the ion KE gain during the ejection process. The dc voltage ramp leads to the natural ion motion to reach the stability diagram boundary at $\beta_z = 0$ and consequently, ions gain kinetic energy. This gain is quite low and thus, the second term in Eq. (3) can be neglected. As displayed in Fig. 5(a), the ion velocity spread is quite important during the ion cloud ejection and varies with q_z. At the high q_z value, the pseudopotential well is deeper and the KE distributions will be broader than those at lower q_z values.

The simulation of ion ejection by dc pulse [case (2), Sect 3.2.2.] gives similar results in term of KE [Fig. 6(b)]. It should be noted that the dc pulse voltage was calculated from QISMS software (Table 2) and was supposed to correspond to ion ejection at $\beta_z = 0$. These q_z, *m/z*, and U_{dc} values were then introduced in SIMION software. As in a dc ramp simulation, a relationship similar to Eq. (3) was found.

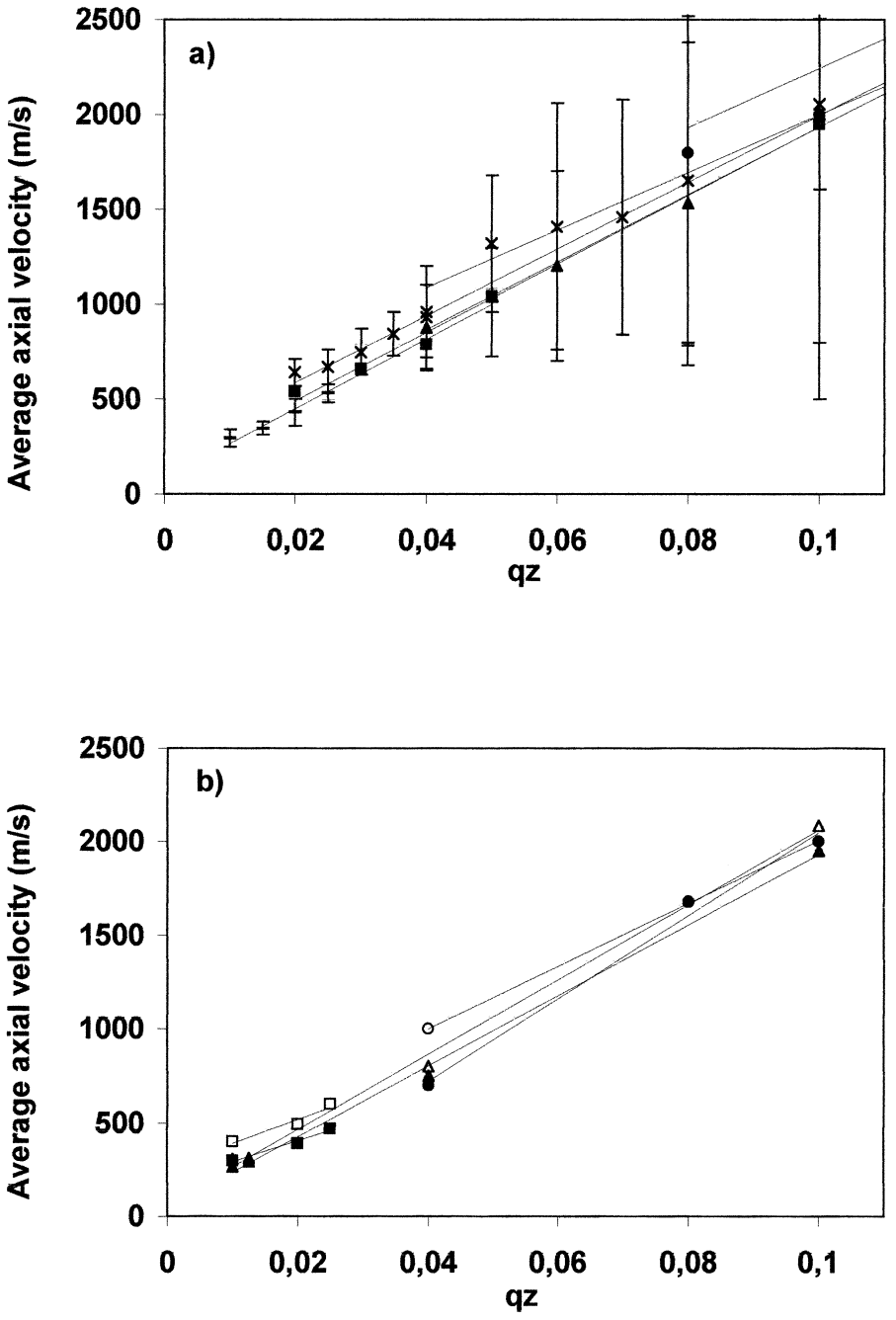

Fig. 5. Average axial velocity obtained by simulation for the dc ramp ($U_{dc} = \alpha t$) ion ejection for different q_z and *m/z* values. Bare lines represent the velocity range (minimal and maximal velocity): (a) dc ramp $\alpha = 10\,000$ V/s: (—) *m/z* 2 000, (■) *m/z* 1 000, (▲) *m/z* 500, (*) *m/z* 200, (×) *m/z* 100, and (●) *m/z* 50. (b) dc ramp $\alpha = 1\,000$ V/s (full symbols) and $\alpha = 5\,000$ V/s (empty symbols): (●) *m/z* 50, (■) *m/z* 200, and (▲) *m/z* 400.

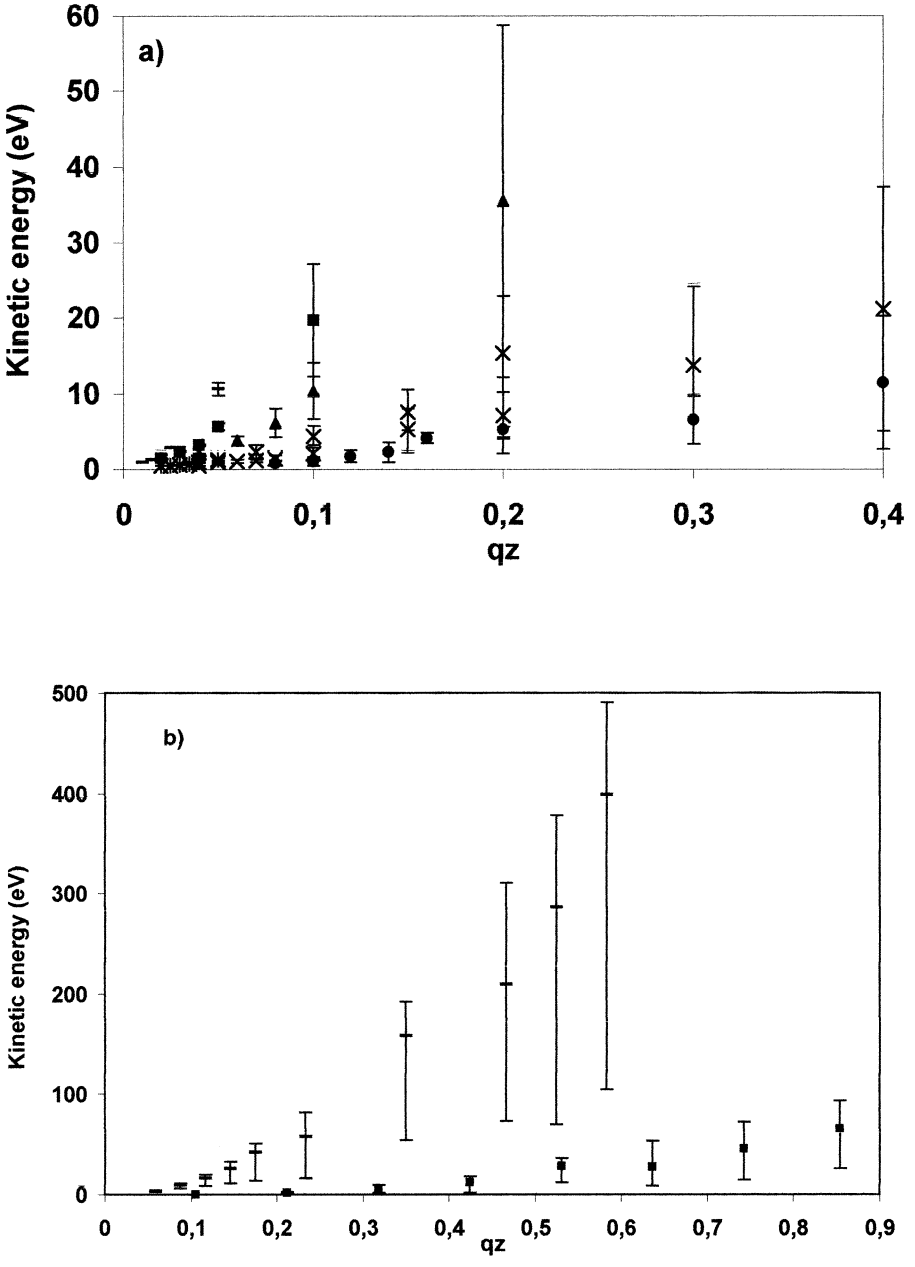

Fig. 6. (a) Average axial KE obtained by simulation of the dc ramp (α = 10 000 V/s) ejection for different q_z and *m/z* values. Bare lines represent the KE range. (—) *m/z* 2 000, (■) *m/z* 1 000, (▲) *m/z* 500, (*) *m/z* 200, (×) *m/z* 100, and (●) *m/z* 50. (b) dc pulse ($U_{dc} = U_0$) simulation at ion ejection of average KE for different q_z and *m/z* values. Bare lines represent the KE range. (—) *m/z* 502 and (■) *m/z* 69.

4.2.2. Experimental exploration

Experimental results on the average ejection ion velocities as a function of the q_z working point for the different *m/z* values are reported in Fig. 7(a). Data provided from simulations are consistent with those obtained from experiments, i.e. a linear relationship between the ion velocity and the q_z value was found. However, the experimental average KE values are

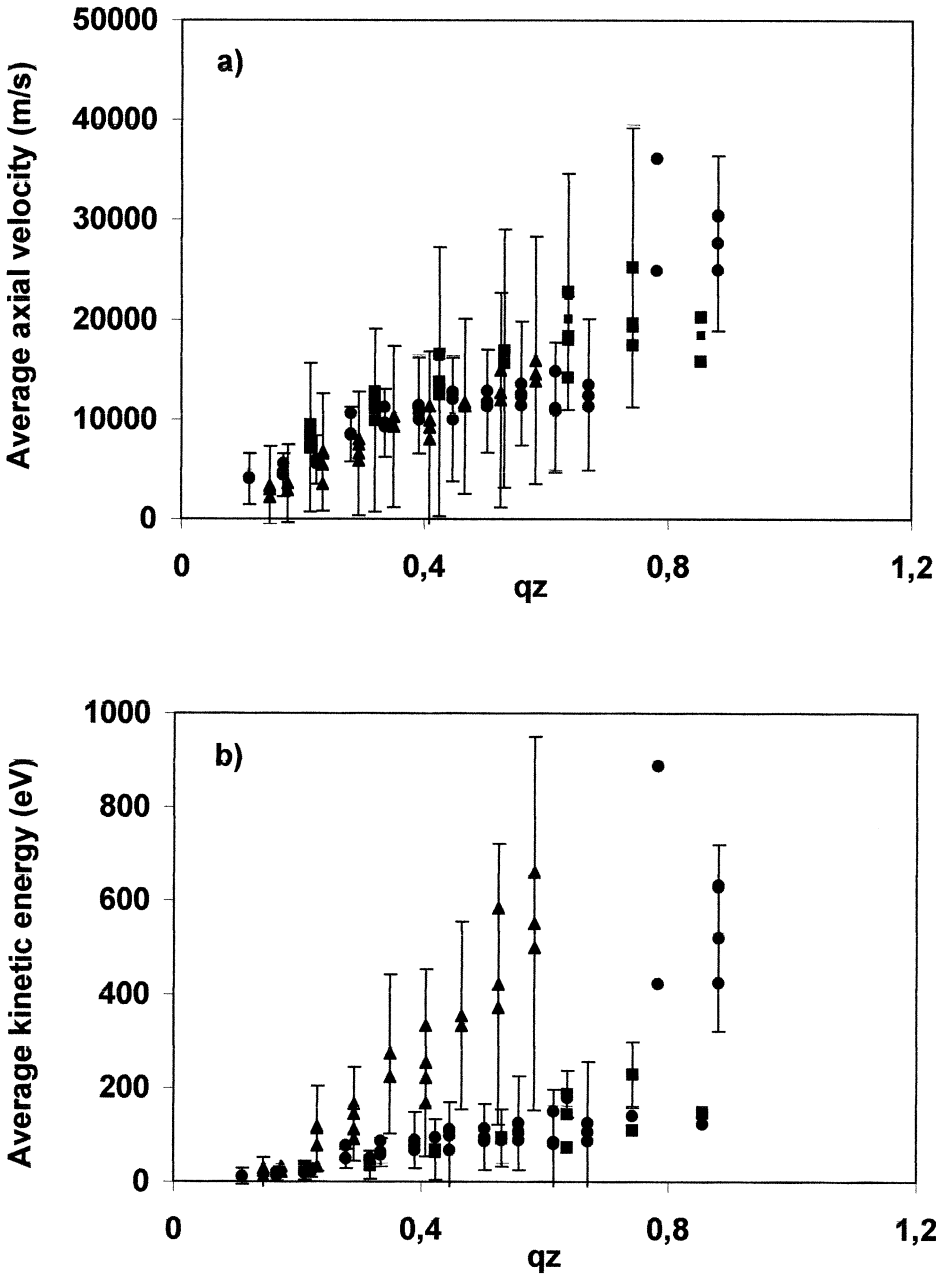

Fig. 7. (a) Experimental measurements of the most probable axial velocity (for ion trap) at ejection (dc pulse voltage $U_{dc} = U_0$) for the different q_z and *m/z* values. Bare lines represent the velocities at FWHM. (▲) *m/z* 502, (●) *m/z* 131, and (■) *m/z* 69. (b) Experimental average axial kinetic energy (ion ejection by dc pulse voltage $U_{dc} = U_0$) when ions are ejected out of the ion trap for different q_z and *m/z* values. Bare lines represent the kinetic energy at FWHM. (▲) *m/z* 502, (●) *m/z* 131, and (■) *m/z* 69.

roughly 1.5 higher than those obtained from the dc pulse simulations. In addition, the KE range is relatively larger than that expected from simulations. For example, at $q_z = 0.6$ (*m/z* 502 of FC-43), the full width at half maximum (FWHM) value of the experimental KE distribution is about 800 eV [Fig. 7(b)], whereas the full KE distribution width provided from simulations in the same conditions is closed to 500 eV [Fig. 6(b)]. This KE variation can be explained by considering that space charge effects are neglected in the simulations and can occur in the present experiments. Indeed, space charge effects imply a more energetic ion cloud due to ion-ion repulsion leading to a higher average KE with a broader distribution after the ejection step. Consequently, the enhanced NLR contributions, which have been observed in this stretched geometry [47,48], modify significantly the ion trajectories by increasing KE and secular frequency [49] for positive ions, leading to higher experimental KE than that provided by simulation, or to losses of ions by NLR.

The comparison of the average axial velocity at the ion trap exit, with those allowed by reTOF/MS will provide the best useful q_z value range. Furthermore, the simulations highlighted that the ion KE range consistent for reTOF analysis require $q_z < 0.1$. Moreover, ions must leave the ion trap cell with the similar KE values for reaching efficient ion detection after flight through the considered IT/O-reTOF/MS tandem. According to our simulations, this condition cannot be achieved for a constant LMCO value during ejection step of the ion cloud (composed by different *m/z* ratios without similar average KE). Thus during the dc ejection step, LMCO has to be adjusted as a function of the *m/z* ratio. Taking into account that the experimental KE distributions are rather large, one could expected that for a constant LMCO value ($q_z < 0.15$), ions could be partially detected during the O-reTOF analysis. In addition, it can be noted that for $q_z < 0.1$, due to a lower pseudopotential depth, the ion cloud size is larger than that it is for higher q_z. Thus, the ion ejection radial velocity increases when q_z decreases (results of simulations not herein reported), and as expected, it affects the ion beam divergence. In that case, an ion beam transfer optic has to be implemented between the ion trap and reTOF mass analyzers, to reduce this beam divergence.

4.3. Condition on ion trap: ejection time

4.3.1. Simulations: ejection by the dc ramp scan

Under the KE conditions suitable for O-reTOF analysis, the ejection time of the different ions has been studied for different working point values. In these simulations, ions are ejected after a cooling time of $t_{toc} = 1000$ μs. The ejection time is defined as the time needed for ion to reach the hole in the end-cap exit (keeping in mind that $t = 0$ is the end of the cooling step). Fig. 8 shows the results of the ion ejection simulation by using two different dc ramps. The observed trend concerning the ejection time is an increase when (1) q_z increases for a given *m/z*, (2) *m/z* increases for a given q_z, and (3) the dc scan rate decreases (both the q_z and *m/z* values are fixed).

4.3.2. Experiments: ejection by dc pulse voltage

Fig. 9 typically illustrates the dependence of the average ejection time (see Sect. 2.2.) upon both the q_z and *m/z* ratio values for different dc pulse voltage values. At constant *m/z* ratio and q_z, the value of the dc pulse voltage was adjusted around the value of dc voltage corresponding to $\beta_z = 0$. This variation strongly influences the ion ejection time, i.e. the higher voltage the lower ejection time. For the lowest dc value, ejection time is closed to 250 μs, excepted for $q_z = 0.42$ (*m/z* 69) and $q_z = 0.15$ (*m/z* 502). For lowest dc pulse voltage than those reported, ions are not ejected. For the highest dc value, the ejection time is very low (<10 μs) whatever the *m/z* and q_z values. The variation of ejection time with dc pulse voltage enlightens that the experimental conditions consistent with ion instability are not well defined in agreement with results of Paradisi [50] and Johnson [51]. At low q_z values (0.15 for *m/z* 502, see Fig. 9), a difference of 7 V in dc pulse voltage involves a variation of 30 μs in average ejection time (from 37 to 66 μs).

It should be noted that the applied dc pulse voltage does not strongly influence the average kinetic energy, i.e. in the previous example, the average KE value is maintained close to 20 eV.

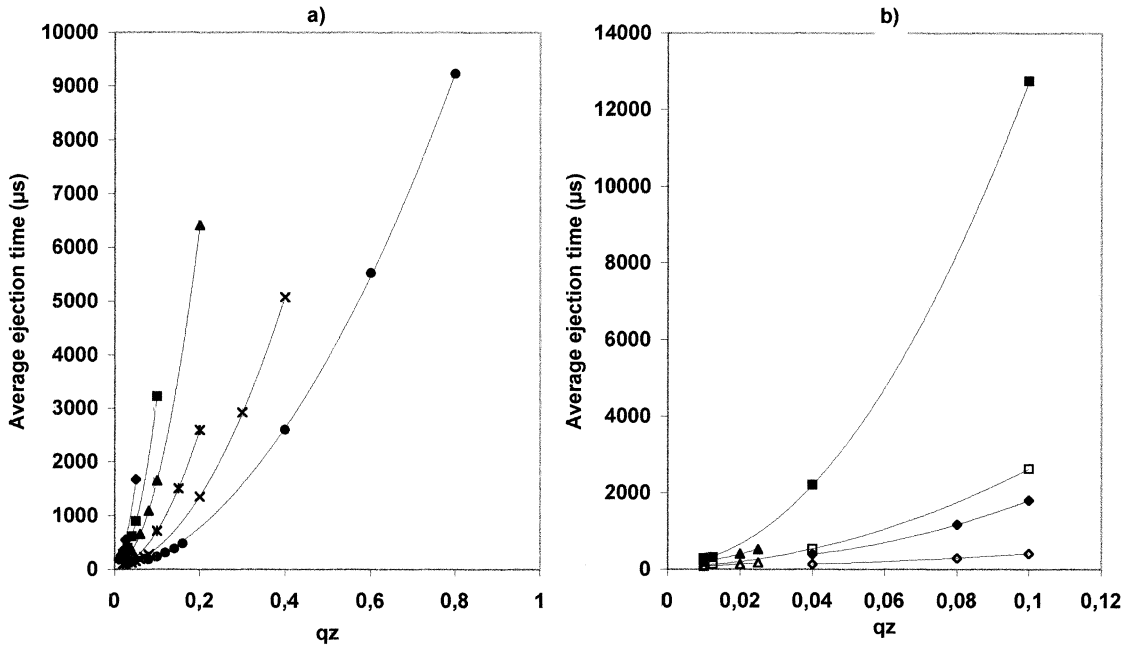

FIG. 8. Average ion ejection time obtained by simulation of dc ramp ($U_{dc} = \alpha t$) ejection, for different q_z and *m/z* values (after a cooling time of 1 000 μs). (a) dc ramp α = 10 000 V/s: (—) *m/z* 2 000, (■) *m/z* 1 000, (▲) *m/z* 500, (*) *m/z* 200, (×) *m/z* 100, and (●) *m/z* 50. (b) dc ramp α = 1 000 V/s (full characters) and α = 5 000 V/s (empty characters): (●) *m/z* 50, (▲) *m/z* 200, and (■) *m/z* 400.

4.3.3. Simulation: ejection by dc pulse voltage

Simulation of the ion ejection performed by the dc pulse application was done with similar conditions as in the previous experiments. The results (not reported herein) display similar trends. Indeed, when the dc voltage increases and the instability $\beta_z = 0$ line is reached, the ejection time decreases and lies in the microsecond range. However, in these simulations, the lowest voltage that permits ion ejection, does not strongly depend upon the q_z and *m/z* values. In that case, the average ejection time is close to 500 μs after applying an adequate dc pulse voltage. The difference between experiments and simulation for the lowest dc pulse voltage can be found in the experimental detection mode, not including the counting mode. For the largest time distribution, the ion current intensity is too low to give a significant signal.

4.3.4. Ion trajectory overlapping

The ion velocity and ejection time ranges obtained from both the simulations and experiments, allow us to estimate the distance, between the end-cap exit and the O-reTOF extraction region, consistent with a simultaneous analysis of the set of ions. These parameters were used to calculate the axial positions and time distributions of analyzed ions after the ion ejection step. Examples of snapshots of the ion beam positions are reported in Figs. 10 and 11. Fig. 10 (ion trajectories after ion ejection by application of the dc ramp from simulation results) shows that for two LMCO values, an overlapping of the different ion beams (i.e. *m/z* 50, *m/z* 100, and *m/z* 200) can be found in the range of 10.6–14.2 cm from the end-cap exit. Moreover, the time range required for the different ions to flight until O-reTOF extraction source (i.e. 20 cm after the ion trap) is about 40 μs. In that case, the triggering of the O-reTOF extraction pulse is not straight forward due to the strong variation of the ion ejection time with the q_z values. In addition, in the previously mentioned O-reTOF/MS analysis conditions and the studied *m/z* range, the expected TOF range is close to 300 μs. In that case, the sampling of

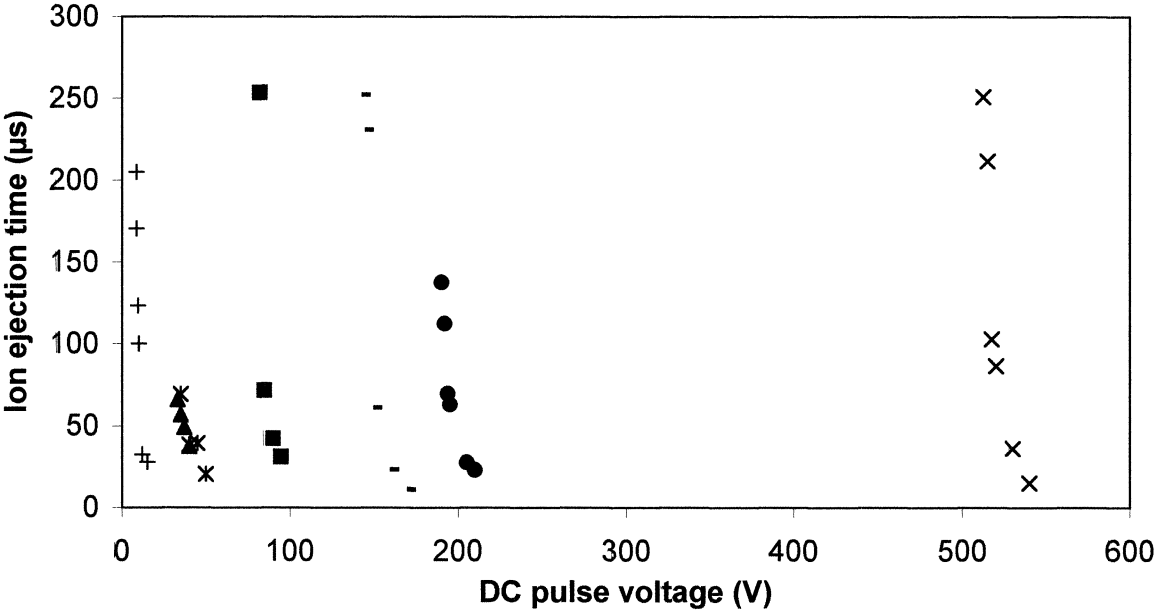

Fig. 9. Experimental average time of ejection evolution with dc pulse voltage at different q_z and for two *m/z* values. For *m/z* 69, the different q_z values were (+) 0.21, (*) 0.42, (■) 0.63, (▲) 0.85. For *m/z* 502, (—) 0.14, (●) 0.35, and (×) 0.58.

the ion beam cannot be realized. Fig. 11 shows the possible ion trajectory overlapping (e.g. *m/z* 69 and *m/z* 502 of FC-43) after the dc pulse ejection step using the experimental ion velocities and ejection time. For a constant LMCO value, two different dc voltages, the highest and lowest voltages (see Sect. 4.3.2.) that permit ejection around $\beta_z = 0$, were used. The time spread between the first and the last ejected

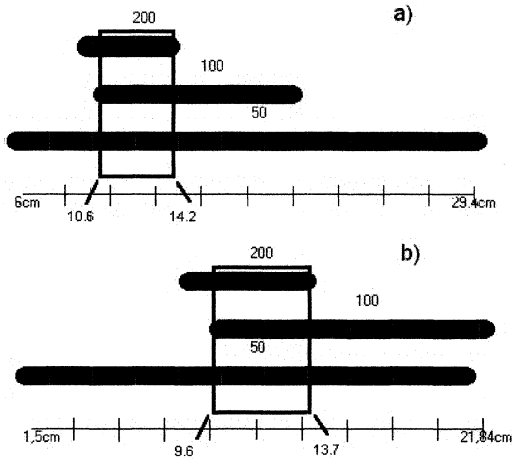

Fig. 10. Ion trajectories overlapping after dc ramp (10 000 V/s) from simulation results, at the total ejection time 275 μs between the first and last ejected ion (*m/z* 50, 100, and 200). (a) The working point of the lowest *m/z* ratio (50 Th) is $q_z = 0.08$. (b) The working point of the lowest *m/z* ratio (50 Th) is $q_z = 0.1$.

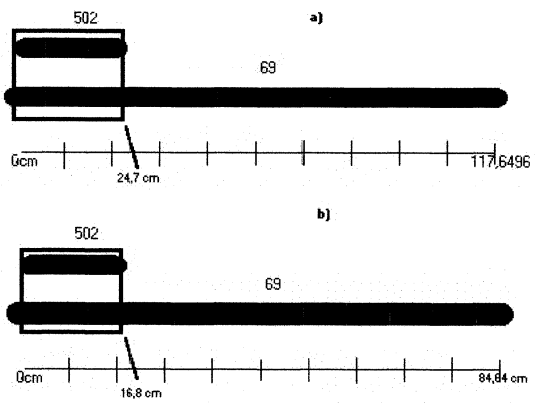

Fig. 11. Ion trajectories (*m/z* 69 and 502) overlapping after dc pulse ejection from experimental results (working point of the lowest *m/z* ratio (69 Th) is $q_z = 0.08$.) (a) For the lowest dc pulse voltage permitting ion ejection: overlapping at the total ejection time 660 μs between the first and the last ejected ion. (b) For the highest dc pulse voltage permitting ion ejection: overlapping at the total ejection time 300 μs between the first and the last ejected ion.

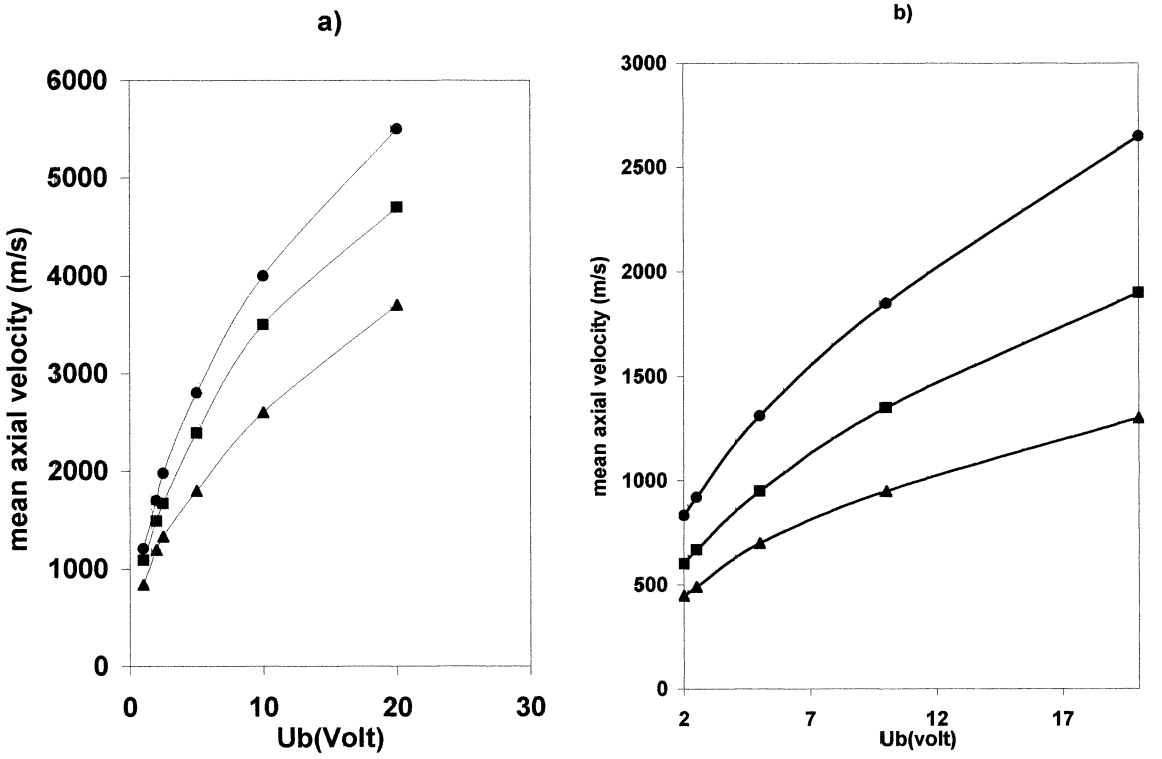

Fig. 12. Simulations of ion ejection by application of dc pulse voltage on end-caps (switching off the drive rf voltage) of mean KE for different *m/z* values. $U_a = -U_b$ (see Fig. 2). (a) (●) *m/z* 50, (▲) *m/z* 100, and (■) *m/z* 200. (b) (●) *m/z* 500, (▲) *m/z* 1 000, and (■) *m/z* 2 000.

ions strongly depend upon the dc pulse voltage, 660 and 300 μs for the lowest and highest dc pulse voltage, respectively. In that case, the experimental synchronization between the ion ejection step and the O-reTOF extraction cannot be optimized for the entire *m/z* ratio range analysis in only one O-reTOF extraction pulse. A sampling of the ejected pseudo-continuous ion beam from ion trap, by a high frequency pusher implemented on the extraction lens of O-reTOF/MS, could be a more realistic solution. This solution does not require synchronization between ion ejection and reTOF analysis. For each ion ejection cycle, 2 or 3 O-reTOF scans can be implemented. Obviously, better results on sensitivity would likely need a greater number of ion ejection cycles. Statistically, it would be possible to analyze the ejected ions of the different species and to rule out discrimination.

4.4. An alternative

In the case of ion beam sampling, ion ejection by the dc pulse applied to the end-cap electrodes with switching off the rf voltage was simulated. Fig. 12 shows the average velocity of different ions for different dc pulse voltages applied to end-caps (seen in Sect. 2). In this configuration, the average KE depends upon the applied field, as expected. It can be noted that this average KE is not strongly dependent upon the q_z value (results not shown). Again, the ejection time and the average ion velocity allow us to expect a pseudocontinuous beam. From these results, the best solution would be a sampling of the ejected ion beam by a high frequency pusher implemented on the extraction lens of O-reTOF/MS.

5. Conclusions

Different ejection modes have been explored to find the best ion ejection conditions from the ion trap cell that are consistent with the use of the O-reTOF analysis. The ion ejection by application of dc scan or dc pulse permits us to obtain a KE range consistent with the considered reTOF analysis for $q_z < 0.15$. However, the use of such low q_z can reduce ion trapping efficiency. At these used q_z values, the corresponding pseudopotential depths are too weak, resulting into an enlargement of the ion cloud, due to charge space effect. Ions will gain KE and the spatial excursions will be larger. Consequently, ions that are affected by these excursions are destabilized by a nonlinear electric field, implying a partial loss of ion cloud and will reduce the trapping efficiency. The ion ejection by application of the dc pulse voltage applied to end-caps, with switching off the driving rf voltage, can be an alternative. But, to reduce ion beam divergence from the end-cap exit, ion optics have to be implemented to increase its transmission. Thus, improvement of the transfer optics such as hexapole, einzel lenses are in progress to reduce the ion beam divergence and to increase the ion transmission. As it has shown from all the experimental results, the ejection time is a quite uncontrollable parameter, which depends too much upon the ion ejection parameters. In that case, the triggering between both ion trap and reTOF/MS is rather impossible. The most appropriate method, considering that the ion beam is rather continuous, is a sampling of this beam, similar to what is done in orthogonal reTOF coupling. For enhancing the duty cycle of the proposed system, the challenge is then to optimize ion ejection (in time and in velocity) to get an ion beam as continuous as possible. In that case, the obtained pseudocontinuous beam of large duration, more than 600 μs, can be sampled by the high frequency pusher.

Acknowledgements

The authors acknowledge gratefully the financial support of MGP Instrument, CNRS, DGA, and P. and M. Curie University. The authors wish to thank Varian Inc. and Bruker for the capable assistance they received from the entire technical staff.

References

[1] A. Fox, S.L Morgan, L. Larsson, G. Odham, Analytical Microbiology Methods Chromatography and Mass Spectrometry, Plenum, New York, 1990.
[2] C. Fenselau, Mass Spectrometry for the characterization of Microorganisms ACS Symposium Series 541, American Chemical Society, Washington, D.C. 1994.
[3] S. Letarte, M. Mousselmad, D. Faubert, M.J. Bertrand, Proceedings of the 46th ASMS Conference on Mass Spectrometry and Allied Topics, Orlando, FL, 1998.
[4] J.P. Anahalt, C. Fenseleau, Anal. Chem. 47 (1975) 219.
[5] D.N. Deller, R.J. Cotter, C. Fenseleau, O.M. Uy, Anal. Chem. 59 (1987) 2806.
[6] T.C. Cain, W.J. Weber, D.M. Lubman, Rapid Commun. Mass Spectrom. 8 (1994) 1026.
[7] T. Krishnamurthy, P.L. Ross, U. Rajamani, Rapid Commun. Mass Spectrom. 10 (1996) 883.
[8] D. Despeyroux, P.Watts, J. Defence, Science 2 (1996) 298.
[9] M.W. Wensing, K.S. Heroux, A.P. Snyder, Proceedings of the 46th ASMS Conference on Mass Spectrometry and Allied Topics, Orlando, FL, 1998.
[10] J.R. Yates III, Electrophoresis 19 (1998) 893.
[11] P.A. Demirev, Y.-P. Ho, V. Ryzhov, C. Fenseleau, Anal. Chem. 71 (1999) 2732.
[12] D.N. Perkins, D.J.C. Pappin, D.M. Creasy, J.S. Cottrell, Electrophoresis 20 (1999) 3551.
[13] K.R. Clauser, P. Baker, A.L. Burlingame, Anal. Chem. 71 (1999) 2871.
[14] A.D. Hendricker, C. Abbas-Hawks, F. Basile, K.J. Voorhees, Proceedings of the 46th ASMS Conference on Mass Spectrometry and Allied Topics, Orlando, FL, 1998.
[15] M. Henchman, C. Steel, J. Chem. Ed. 75 (1998) 1042.
[16] G. Matz, A. Harder, A. Schillings, P. Rechenbach, Proceedings of the 46th ASMS Conference on Mass Spectrometry and Allied Topics, Orlando, FL, 1998.
[17] M.R. Green, R.H. Bateman, R. Carruthers, A.J. Gilbert, A. Preston, Proceedings of the 46th ASMS Conference on Mass Spectrometry and Allied Topics, Orlando, FL, 1998.
[18] S.A. Ecelberger, R.J. Cotter, T.J. Cornish, C. Fenselau, W.A. Bryden, Proceedings of the 45th ASMS Conference on Mass Spectrometry and Allied Topics, Palm Springs, CA, 1997.
[19] R.J. Cotter, C. Fancher, T.J. Cornish, J. Mass Spectrom. 34 (1999) 1368.
[20] A.N. Krutchinsky, A.V. Loboda, V.L. Spicer, R. Dworschak, W. Ens, K.G. Standing, Rapid Commun. Mass Spectrom. 12 (1998) 508.
[21] A.V. Loboda, A.N. Krutchinsky, M. Bromirski, W. Ens, K.G. Standing, Rapid Commun. Mass Spectrom. 14 (2000) 1047.
[22] J.H.J. Dawson, M. Guilhaus, Rapid Commun. Mass Spectrom. 3 (1989) 155.

[23] J.M. Campbell, B.A. Collings, D.J. Douglas, Rapid Commun. Mass Spectrom. 12 (1998) 1463.
[24] C. Weickhardt, C. Lifshitz, Eur. Mass Spectrom. 1 (1995) 223.
[25] K.P. Aicher, M. Muller, U. Wilhem, J. Grotemeyer, Eur. Mass Spectrom. 1 (1995) 331.
[26] S.M. Michael, M. Chien, D.M. Lubman, Rev. Sci. Instrum. 63 (1992) 10.
[27] P. Kofel, M. Stockli, J. Krouse, U.P. Schlunegger, Rapid Commun. Mass Spectrom. 10 (1996) 658.
[28] W.M. Doroshenko, R.J. Cotter, J. Mass Spectrom. 33 (1998) 305.
[29] R.W. Purves, L. Li, J. Am. Soc. Mass Spectrom. 8 (1997) 1085.
[30] B.M. Chien, S.M. Michael, D.M. Lubman, Rapid Commun. Mass Spectrom. 7 (1993) 837.
[31] A. Alili, J. Andre, F. Vedel, Phys. Scr., T 22 (1988) 325.
[32] M. Schubert, I. Siemers, R. Blatt, Appl. Phys. B 51 (1990) 414.
[33] H.P. Reiser, R.E. Kaiser, P.J. Savickas, R.G. Cooks, Int. J. Mass Spectrom. Ion Processes 106 (1991) 237.
[34] J.F.J. Todd, A.D. Penman, R.D. Smith, Int. J. Mass Spectrom. Ion Processes 106 (1991) 117.
[35] G.E. Patterson, E.R. Badman, A.L. Schreiweis, J.M. Wells, R.G. Cooks, Proceedings of the 47th ASMS Conference on Mass Spectrometry and Allied Topics, Dallas, TX, 1999.
[36] D.A. Dahl, Proceedings of the 43rd ASMS Conference on Mass Spectrometry and Allied Topics, Atlanta, GA, 1995, p. 717.
[37] J.C. Mathurin, T. Faye, A. Brunot, J.C. Tabet, G. Wells, C. Fuché, Anal. Chem. 20 (2000) 5055.
[38] B. Bolton, G. Wells, M. Wang, Proceedings of the 41st ASMS conference on Mass Spectrometry and Allied Topics, San Francisco, CA, 1993.
[39] W.C. Wiley, I.H. McLaren, Rev. Sci. Instrum. 26 (1955) 1150.
[40] L. He, D.M. Lubman, Rapid Commun. Mass Spectrom. 11 (1997) 1467.
[41] R.K. Julian, M. Nappi, C. Weil, R.G. Cooks, J. Am. Soc. Mass Spectrom. 6 (1995) 57.
[42] M.W. Forbes, M. Sharifi, T. Croley, Z. Lausevic, R.E. March, J. Mass Spectrom. 34 (1999) 1219.
[43] H. Bui, R.G. Cooks, J. Mass Spectrom. 33 (1998) 297.
[44] F.A. Londry, R.L. Alfred, R.E. March, J. Am. Soc. Mass Spectrom. 4 (1993) 687.
[45] R.E. March, M. Tkacyzk, F.A. Londry, R.L. Alfred, Int. J. Mass Spectrom. Ion Processes 125 (1993) 9.
[46] F.G. Major, H.G. Dehmelt, Phys. Rev. 179 (1968) 91.
[47] J. Louris, J. Schwartz, G. Stafford, J. Syka, D. Taylor, Proceedings of the 40th ASMS conference on Mass Spectrometry and Allied Topics, Washington, DC, 1992.
[48] V. Steiner, C. Beaugrand, P. Liere, J.-C. Tabet, J. Mass Spectrom. 34 (1999) 511.
[49] M. Spendore, F.A. Londry, R.E. March, R.J.S. Morrison, P. Perrier, J. André, Int. J. Mass Spectrom. Ion Processes 156 (1996) 11.
[50] C. Paradisi, Org. Mass Spectrom. 27 (1992) 252.
[51] J.V. Johnson, Rapid Commun. Mass Spectrom. 6 (1992) 763.